

Adaptive Pixel-wise Structured Sparse Network for Efficient CNNs

Chen Tang
Tsinghua University

tangc20@mails.tsinghua.edu.cn

Zhuqing Yuan
Tsinghua University
yuanzhuqing@tsinghua.edu.cn

Wenyu Sun
Tsinghua University

wy-sun16@mails.tsinghua.edu.cn

Yongpan Liu
Tsinghua University
ypliu@tsinghua.edu.cn

Abstract

To accelerate deep CNN models, this paper proposes a novel spatially adaptive framework that can dynamically generate pixel-wise sparsity according to the input image. The sparse scheme is pixel-wise refined, regional adaptive under a unified importance map, which makes it friendly to hardware implementation. A sparse controlling method is further presented to enable online adjustment for applications with different precision/latency requirements. The sparse model is applicable to a wide range of vision tasks. Experimental results show that this method efficiently improve the computing efficiency for both image classification using ResNet-18 and super resolution using SRResNet. On image classification task, our method can save 30%-70% MACs with a slightly drop in top-1 and top-5 accuracy. On super resolution task, our method can reduce more than 90% MACs while only causing around 0.1 dB and 0.01 decreasing in PSNR and SSIM. Hardware validation is also included.

1. Introduction

Convolution neural networks (CNNs) have achieved great success for a wide range of computer vision tasks in recent years. However, the high accuracy is often achieved at the cost of heavy memory and computation consumption with deeper and wider CNNs, which prevents it to be applied to embedded devices and real-time applications.

To solve the problem, one way is to use weight pruning methods, which can effectively compress the weight parameters to slim the models. Early methods generate unstructured sparsity [23, 10, 12, 9, 11], which greatly compress the model but is not convenient for hardware deployment. Therefore, more researches focus on learning structured sparsity [24, 17, 29]. Although the weight pruning methods can effectively reduce the model parameters, they are static without considering the spatial redundancy of the image. They

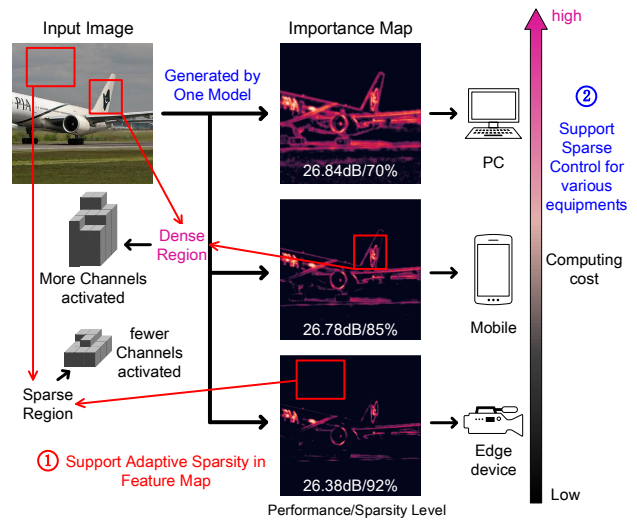


Figure 1. Illustration of our work on image restoration task. An importance map F is generated from the input image to define sparsity for each pixel. Larger magnitude in F , which displays a brighter color, means more numbers of channels are activated in the feature map for the corresponding region. The total network sparsity is controlled through importance maps by a dynamic adjustment mechanism in one model without retraining.

have the same computing cost for different inputs or image regions, and cannot make adaptation spatially, which limits the further improvement of model accuracy.

Recently, dynamic model inference has attracted more attention. They attempt to dynamically allocate the computing resources according to specific requirements and limitations. These methods are input-dependent, which means the computing cost is adaptively changed for different images, even though the image size keeps the same. They can properly allocate more computing resources for the importance regions such as the ROI (Region of Interest) pixels, while pay less attention to the sub-important regions such as the background. Researches [7, 26, 39] first propose several layer-

wise methods to activate different layers for different inputs or distribute different numbers of layers for important and sub-important regions. Then several channel-wise [27, 8] methods are proposed, which can dynamically empty the one whole channel to save computation. To further improve the performance, the more refined pixel-wise [6, 33, 43, 21, 20] methods are proposed. The philosophy is to save only important pixels to compose the feature map. However, the selected pixels tend to be different between layers, which exerts extra overhead for online and offline compiling and not very friendly for hardware implementation. Our method is also pixel-wise based while performs in a different manner. Firstly, we treat pixels differently according to their importance level instead of just discarding those unimportant ones. Pixels in sub-important region can be activated with fewer channels while the important ones more. In this way, our method can maintain better accuracy/latency trade-off. Secondly, The sparsity is determined by an unified importance map, which makes the structure of sparsity invariant from layer to layer. This makes our method easier to deploy on hardware devices than other pixel-wise methods.

Sometimes, it could be necessary to deploy models at different sparse levels on the same device. For example, when the battery is well charged, the model can run with the full use of computing resources. When the battery is running out, models with higher sparse level are needed. Also, different applications can have different power or latency requirements. Previous methods need to train many models offline to cope with this problem, which is inconvenient and time-consuming. Through special design, our method can automatically control the sparse level online in one model, which can be a better solution to cope with the heavy burden of multiple models training.

The main contributions of this paper include:

- 1) We propose a spatially adaptive CNN model to dynamically generate pixel-level sparsity and reduce the storage and computing cost. The sparsity is guided by a unified importance map. An example of hardware implementation is also presented.
- 2) Our method can online control the sparsity level in one model, thus saving the burden to train multiple models for various devices or requirements.
- 3) Our methods can be widely utilized on various vision tasks. We validate the effectiveness on the super resolution and image classification tasks. Experimental results show the proposed models achieve comparable or better performance with state-of-art methods.

2. Related Work

Our method is related with various previous works like structured sparsity pruning and input-dependent execution.

In this section, we briefly introduce static weight pruning and dynamic execution. In weight pruning, network sparsity is generated by pruning the unimportant weights, which results in a static sparse network. While in dynamic execution, the sparsity is generated in an input-dependent manner.

2.1. Static Weight Pruning

Weight pruning is very effective in reducing redundant connections in the model [23, 10, 12, 9, 11]. In particular, structured pruning [24, 17, 29] has gained more and more attention, since the pruned network is more friendly to hardware deployment. Structured pruning can be further divided into filter pruning, channel pruning and kernel shape pruning according to the specific methods [42].

Filter pruning searches for unimportant filters, by pruning which the corresponding output channels can be skipped to generate sparsity [16, 24, 30, 4]. The filters can be selected based on the l_1 -norm of weight channels [24], the statistics information computed from its following layer [30] or the correlation between each filters [4]. Filter pruning can largely reduce the model size but may cause accuracy loss because of its large-grained nature.

Channel pruning searches for unimportant channels to leave out. Thus, filters producing this channel and those related ones in the following layer can be pruned [29, 17, 28, 46, 44]. The pruned channel can be selected based on LASSO regularization [29], reconstruction error before and after pruning [17], generative adversarial learning [28] or an attention mechanism [46].

Kernel Shape pruning or pattern pruning reduces convolution kernels patterns to a limited number, which also generates structured sparsity in kernel-wise. Ma *et al.* [31] propose pattern pruning and force all the 3X3 convolution kernels collapsing into several patterns which only has four non-zero parameters. Wang *et al.* [40] select patterns based on probability density function and design a hardware architecture to better support the algorithm.

Although weight pruning can reduce the model size, its sparsity is static in network inference regardless of the input data. Therefore, some researchers turn to the dynamic execution methods, of which the generated sparsity is input-dependent.

2.2. Dynamic Sparsity Aware Execution

Dynamic Execution methods try to utilize the redundancy existed in the feature map to generated sparsity dynamically. Dynamic execution is further divided into layer-wise, channel-wise and pixel-wise methods.

Layer-wise dynamic execution methods explore to reduce the number of layers to relieve computation burden according to input data [7, 26, 39]. The skipping decision is made based on a halting score that is generated by the input of current layer [7], the classifying difficulty estimated from

pixels [26] or a gate function attached with each layer [39].

Channel-wise dynamic execution methods dynamically inactivate channels so that calculations related with them can be saved. Lin *et al.* [27] use Markov decision process to dynamically prune the channel based on the input. Gao *et al.* [8] uses an attention mechanism to dynamically choose the top-k importance channels to preserve in each layer.

Layer-wise and channel-wise methods skip the computation related to specific layers or channels, which take the sparsity of the input as a whole or average. While it is easy to notice that different inputs have different spatial sparsity. Thus pixel-wise methods are proposed to fill this gap.

Pixel-wise methods try to let fewer pixels involved in the calculation based on the spatial redundancy [6, 33, 43, 21, 20]. One approach is to sample representative or important pixels and process them only. The sampling is done by separating images into background and foreground blocks [33] or by a gumbel-softmax based stochastic sampling module [43]. Another idea is to reduce the number of pixels by down-sampling feature map [21]. The omitted pixel is prone to be scattered in the former methods. Changing the size of the feature map also limits the application in some tasks, such as super resolution, or segmentation. In this work, we propose a pixel-wise structured sparsity network that different numbers of channels are activated for different pixels. Also, our method support online sparse control, which previous methods cannot offer.

3. Proposed Method

The overall framework of the proposed spatially adaptive network is shown in Fig. 2(a), and is composed of two parts: an importance map network and a main functional network. The former one generates an importance map \mathbf{F} , which indicates the importance level of each pixel in the input image. The network is designed to be extremely light-weight. \mathbf{F} is quantized to represent the number of valid output channels for each pixel. The main functional network represents various CNN solutions in a wide range of vision tasks, such as image classification or super-resolution network. Fig. 2(b) illustrates the sparse inference progress. The sparsity in feature map is fully controlled by a unified quantized importance map \mathbf{Q} from \mathbf{F} , and zero blocks can only be in place of latter channels. As a result, the proposed spatially adaptive sparse network is structured for hardware implementation.

3.1. Importance Map Network

The importance map network (IMN) aims at generating a sigmoid activated feature map $\mathbf{F}^{H \times W \times 1}$ to indicate the important regions of the image, which can be illustrated in Eq. 1, where $\psi(\cdot)$ refers to the IMN module.

$$\mathbf{F} = \psi(I_{in}), \quad \mathbf{F}(i, j) \in (0, 1) \quad (1)$$

Regions with lower value in \mathbf{F} are less important, where fewer channels will be allocated to these pixels. To realize such spatial sparsity in the feature map, a binary mask \mathbf{M} is generated from the quantized \mathbf{F} in the training phase.

Specifically, we first quantize the $\mathbf{F}(i, j)$ into $\mathbf{Q}(i, j)$ by L levels with quantization step $S = \lfloor C/L \rfloor$, where C is the number of channels in the original dense feature map.

$$\mathbf{Q}(i, j) = l - 1, \quad \frac{l-1}{L} \leq \mathbf{F}(i, j) < \frac{l}{L}, \quad l = 1, \dots, L \quad (2)$$

Then we generate the binary mask \mathbf{M} according to the quantized \mathbf{Q} . For each pixel $m = \mathbf{M}(i, j) \in \mathbb{R}^{1 \times C}$, it can be denoted as Eq. 3. With higher $\mathbf{Q}(i, j)$, more channels for pixel (i, j) are activated.

$$m(k) = \begin{cases} 1, & k \leq S \times \mathbf{Q}(i, j) \\ 0, & k > S \times \mathbf{Q}(i, j) \end{cases} \quad (3)$$

Since the operation of quantization in Eq. 2 is non-differential, we adopt a **tanh** function to approximate the gradient propagation, which enables the whole network can be end-to-end trained. As a result, Eq. 2 and Eq. 3 can be combined together as Eq. 4. The **sign** function binarizes the input into $\{0, 1\}$ and keeps the gradients from output to input unchanged. α is a scale factor to control the gradient magnitude, which is set for 4 in our paper. During training, \mathbf{M} makes dot product with the output of each convolution layer to force the feature map to be sparse. The zero blocks are skipped to reduce the computing costs in inference phase.

$$m(S \times l : S \times l + S) = \mathbf{sign}(\mathbf{tanh}(\alpha \times (\mathbf{F}(i, j) - \frac{l}{L}))) \quad (4)$$

3.2. Integrated with different CNN blocks

The computed binary mask \mathbf{M} can be integrated into multiple kinds of CNN modules to generate sparsity in the feature map. Fig. 3 shows how to generate \mathbf{M} in multiple common cases during training. In ResNet, all convolution outputs make dot product with \mathbf{M} after the skipping connection. In This way, the sparse structure in the output feature map will not be destroyed. In layers that input and output have different numbers of channels, two different masks \mathbf{M}_1 and \mathbf{M}_2 are needed. They can both be quantized from the importance map \mathbf{F} ahead. In some cases, the spatial scales of the feature map may change, like the up-sample operation in super resolution tasks or pooling layers in classification tasks. To ensure \mathbf{M} can have identical shape, one choice is to resize \mathbf{F} through extra convolution layers. Another solution is to directly up-sampling (e.g., nearest interpolation) or pooling (e.g., max pooling) \mathbf{F} to make the spatial size compatible with the feature map. In real implementation, we find the latter method can achieve better performance with less computing cost. The claim will be discussed in the section of ablation study.

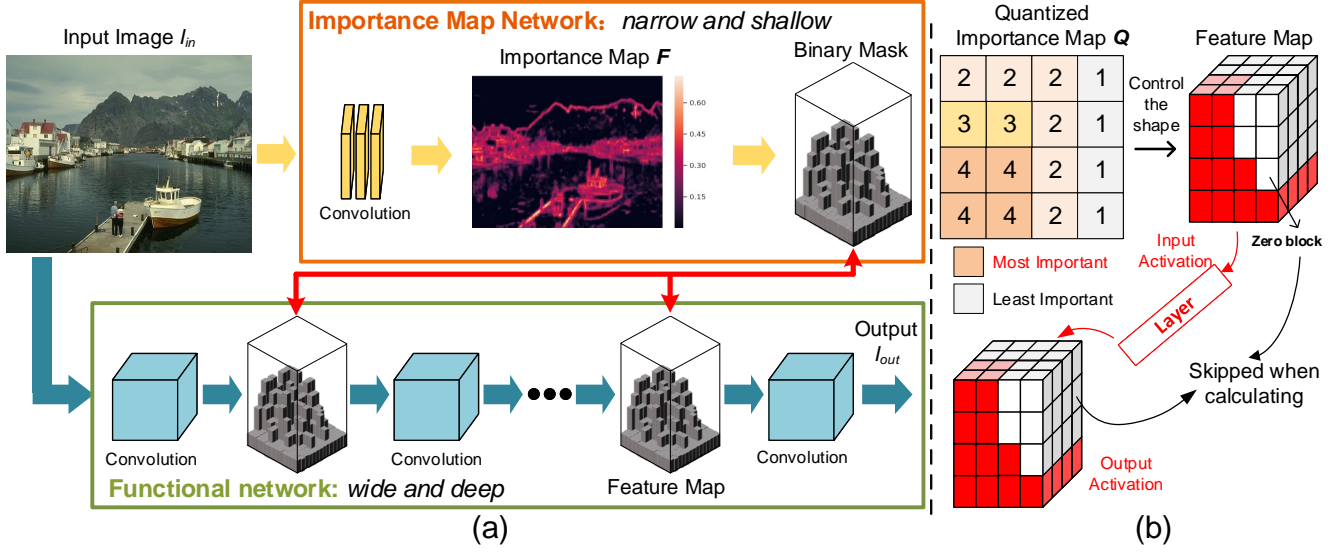


Figure 2. (a) Overview of Our Method. The mask is first generated and all the intermediate feature maps will share the same shape with it (b) A Detailed View of Activation Sparsity. The quantization mechanism is explained in Section. 3.1. Activation Sparsity is the sparsity along the channel dimension.

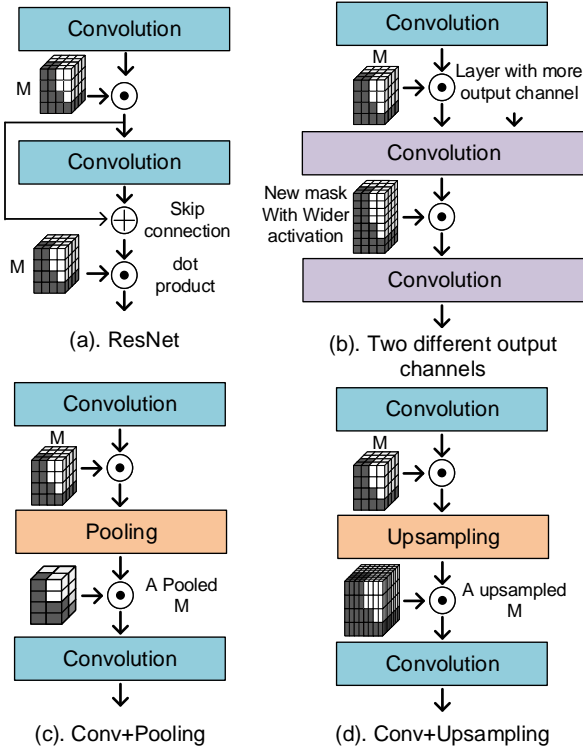


Figure 3. Integrating binary mask M with different CNN blocks.

3.3. Spatially Sparse Controlling

Based on the trainable IMN module, the next question is how to successfully train a valid importance map F . The

training of F relies on our loss function, which will be first presented. Then we further consider an optimizing method to make the model sparsity controllable, where implementation of our Automatic Sparse Controlling (ASC) module and the change of the loss function will be introduced.

Loss function. The loss function \mathcal{L}_{total} is denoted in Eq. 5, which is composed by two parts: the original loss function \mathcal{L}_{main} for the main functional network and the regularization term $\mathcal{L}_{sparse} = |l_1(F) - \gamma|$ from the IMN module, where l_1 is the l_1 -norm function. \mathcal{L}_{main} can be the cross entropy loss for classification task, the L1/L2 loss for the super-resolution task, or some others. The \mathcal{L}_{sparse} aims to make the model sparse. Optimizing \mathcal{L}_{main} and \mathcal{L}_{sparse} is an adversarial process. The balanced point is controlled by the hyper-parameter λ and γ . The final model tends to be more sparse with larger λ and smaller γ . With such defined \mathcal{L}_{total} , the two network can be optimized together to trade off the accuracy and the sparse level properly and adaptively. In this way, we can train a model without ASC module.

$$\mathcal{L}_{total} = \mathcal{L}_{main} + \lambda \mathcal{L}_{sparse} \quad (5)$$

Automatic Sparse Controlling. Pruning multiple models with various sparse levels is inconvenient and time-consuming when the accuracy/latency requirements change. A straightforward way is to manually increase or decrease each value in Q to adjust the the number of activated channels. However, it is hard to decide which pixel should be changed to promise the final accuracy. Therefore, an ASC module is designed to learn where to adjust Q is better and how to control the amount of change in sparse level.

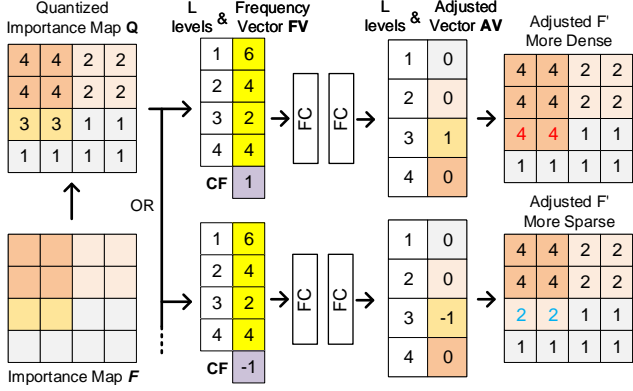


Figure 4. Illustration of the automatic sparse controlling method.

Since the importance level of these pixels has already been measured by the IMN module, there is no need to reinvent the wheel by adjusting Q pixel by pixel. In addition, Q is quantized from F and it can be observed that pixels with same quantization levels are prone to gather together. Therefore, we try to do same change to pixels with same value in Q (e.g. add them by one for all). In order to control the amount of total change in sparsity, the frequency of occurrence for each quantization level is needed. Also, an extra signal called control factor (CF) that indicates the change direction is considered. The total procedure is shown in Fig. 4. Firstly, the statistical frequency for each value is counted to compose a 1-D tensor denoted as the frequency vector FV . Then, an adjusted vector AV is generated from the concatenation of FV and CF to indicate the adjusting weight for different L regions. The total adjustment in sparse level and the process can be formulated by Eq. 6.

$$\begin{aligned} \Delta l_1(F) &= l_1(F') - l_1(F) = FV^T \cdot AV \\ &= FV^T \cdot \varphi(FV, CF) \end{aligned} \quad (6)$$

During training, we randomly generate an integer CF , e.g., $CF \in \{-2, -1, 0, 1, 2\}$. Each CF represents each sort of sparse adjustment. To make the adjustment controlled by CF , the \mathcal{L}_{sparse} in this mode can be redefined in Eq. 7, where β means the targeted sparse change. β is controlled by CF , e.g., $\beta = 0.1$ for $CF = 1$ and $\beta = -0.1$ for $CF = -1$. In this way, we can directly choose different values of CF in inference phase to online obtain different sparse levels. The total procedure is summerized in Algorithm 1. We show in ablation study that the ASC module can effectively adjust the sparse level online and perform better the straightforward method.

$$\mathcal{L}_{sparse} = |l_1(F) - \gamma| + |\Delta l_1(F) - \beta| \quad (7)$$

Algorithm 1 Sparse Controlling Flow

- 1: \mathbb{S} : set of CF . $\psi()$: IMN network. $\varphi()$: ASC network.
 $\phi()$: main functional network. FP : feature map
- 2: **repeat**
- 3: Fetch a training mini-batch x
- 4: $F = \psi(x)$, $Q = \text{Quantize}(F)$
- 5: Randomly choose CF from \mathbb{S} , $\beta \leftarrow CF$
- 6: $FV \leftarrow Q$, $AV = \varphi(FV)$
- 7: Generate adjusted F' from F and AV
- 8: $M \leftarrow F'$
- 9: $\mathcal{L}_{main} = \text{loss}(\phi(FP \cdot M), \text{labels})$
- 10: Generate \mathcal{L}_{sparse} by Eq. 6 and 7
- 11: $\mathcal{L}_{total} = \mathcal{L}_{main} + \lambda \mathcal{L}_{sparse}$
- 12: Back propagation and update parameters
- 13: **until**
- 14: Iters reaches desired maximum

4. Experiment

Our methods can be utilized on multiple applications. Super resolution (SR) and Image classification tasks are chosen to validate our design. The size of the feature maps in SR network is gradually increased while it is reduced for the classification network. Therefore, the two tasks are representative enough to include all common-used CNN blocks.

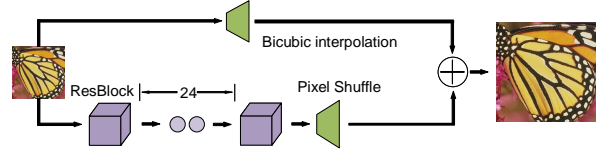


Figure 5. Baseline Model for Super Resolution

4.1. Super Resolution

Experimental setup. We apply our method on the classic single image super resolution (SISR) task and the baseline model is SRResNet [22]. We set adequate 24 Res-Blocks and increase the channel number to 128 in intermediate layers, which results in more than 1000G operations of multiply and accumulate (MACs) for the dense model. The spatially sparse models using proposed method are trained on the widely used DIV2K [38] dataset for the 2X scaling up task. The results are measured on four standard benchmarks, including Set5 [2], Set14 [45], BSD100 [32] and Urban100 [19]. Peak signal to noise ratio (PSNR) and structural similarity index (SSIM) [41] are adopted as the evaluation criteria. The binary mask M is applied to every intermediate feature map except for the last layer that generates the 3-channel output images. Adam optimizer and $2e-4$ learning rate is adopted for all models. We set $\lambda = 2.5e-3$ and let the sparse controlling factor CF to be randomized in $\{0, 1, 2, 3\}$ during

Table 1. Comparison between our models with other state-of-the-art light-weight methods for SRx2. The best and sub-best performance is highlighted in red and blue. MACs is computed in average when the original HR images are 720P

Method	MACs	Set5		Set14		B100		Urban100	
		PSNR	SSIM	PSNR	SSIM	PSNR	SSIM	PSNR	SSIM
FSRCNN[5]	6.0G	37.00	0.9558	32.63	0.9088	31.53	0.8920	29.88	0.9020
DRRN[36]	6796.9G	37.74	0.9591	33.23	0.9136	32.05	0.8973	31.23	0.9188
MemNet[37]	623.9G	37.78	0.9597	33.28	0.9143	32.08	0.8978	31.31	0.9195
SelNet[3]	225.7G	37.89	0.9598	33.61	0.9160	32.08	0.8984	-	-
CARN[1]	222.8G	37.76	0.9590	33.52	0.9166	32.09	0.8978	31.92	0.9256
OISR-RK2-s[14]	316.2G	37.98	0.9604	33.58	0.9172	32.18	0.8996	32.09	0.9281
OISR-LF-s	316.2G	38.02	0.9605	33.62	0.9178	32.20	0.9000	32.21	0.9290
Ours($\lambda=1e-4$)	352G	37.95	0.9605	33.41	0.9180	32.21	0.9000	31.42	0.9325
Ours($\lambda=5e-4$)	209G	38.00	0.9606	33.38	0.9182	32.22	0.9002	31.49	0.9328
Ours($\lambda=2.5e-3$)	30.5G	37.88	0.9599	33.30	0.9164	32.11	0.8985	31.21	0.9284
Ours-ASC(CF=0)	72.2G	37.90	0.9599	33.36	0.9165	32.14	0.8984	31.36	0.9293
Ours-ASC(CF=1)	112.5G	37.95	0.9602	33.42	0.9171	32.17	0.8993	31.47	0.9317
Ours-ASC(CF=2)	174.5G	37.97	0.9604	33.44	0.9175	32.19	0.8996	31.51	0.9324
Ours-ASC(CF=3)	262.1G	37.99	0.9605	33.45	0.9178	32.20	0.8998	31.52	0.9328
MSRN[25]	1356.8G	38.08	0.9605	33.74	0.9170	32.23	0.9013	32.22	0.9326
Baseline	1770.6G	38.12	0.9611	33.60	0.9194	32.27	0.9010	31.92	0.9374

Table 2. Comparison between our model and other pruning or execution methods in ResNet-18.

Method	Type	Top1 Acc	Top5 Acc	Mac Saving
SFP[15]	weight pruning	3.18↓	1.85↓	1.72X
NS[29]	weight pruning	1.77↓	1.29↓	1.39X
DACP[46]	weight pruning	2.29↓	1.38↓	1.89X
FPGM[16]	weight pruning	1.87↓	1.15↓	1.72X
LCCL[6]	pixel-wise	3.65↓	2.30↓	1.53X
CGNN[18]	layer-wise	1.62↓	1.03↓	1.61X
FBS[8]	channel-wise	2.54↓	1.46↓	1.98X
ours($\lambda = 1e - 1$)	pixel-level	0.14 ↑	0.44↑	1.39X
ours($\lambda = 2.5e - 1$)	pixel-level	0.75 ↓	0.2 ↓	1.85X
ours($\lambda = 3e - 1$)	pixel-level	1.41↓	0.74↓	2.08X
ours-ASC(CF=1)	pixel-level	0.90↓	0.25↓	1.62
ours-ASC(CF=0)	pixel-level	0.95↓	0.32↓	1.75
ours-ASC(CF=-1)	pixel-level	1.12↓	0.37↓	1.84

Table 3. Different structures of importance map network

Structure of IMN module	Mac Saving	results for PSNR		
		Set5	Set14	BSD100
6 Conv, 32 channel (8.7G)	22.0X	37.91	33.42	32.17
4 Conv, 32 channel (4.5G)	22.6X	37.91	33.41	32.16
4 Conv, 64 channel (17.5G)	18.5X	37.92	33.47	32.20
3 Conv, 64 channel (9.0G)	16.7X	37.99	33.49	32.20

training to support automatic sparse controlling within one model. The γ is set for 0.2 in Eq. 7. Several models without the equipment of ASC module are also trained, which use different λ settings. We compare our method with several light-weight SR networks [5, 36, 37, 3, 14, 25]

Test results The final reconstruction accuracy and computing costs are listed in Table. 4 in various datasets. When compared to the baseline model, the proposed method can dramatically save the computation cost by reducing more than 90% MACs while only causing around 0.1 dB decreasing in PSNR and less than 0.01 SSIM drop. The model tested with four controlling factors CF achieves compara-

ble or even better performance with fewer computing costs. We are better for SSIM on most of the conditions. A clear PSNR/MACs trade-off is shown on Fig. 6. Our model also supports ultra efficient inference when CF reach its least while the PSNR or SSIM are still promised. Therefore, it can be adopted for real-time applications to reduce latency. Moreover, our method can be rapidly deployed on various embedded systems with different computing power without retaining new models. The CF can control the sparse level easily, which is convenient for freely development.

4.2. Image Classification

Experimental setup. We further validate our method on another typical vision task of image classification. ResNet-18 [13] is set as the baseline model. We train the models on the official ImageNet dataset [34]. The baseline ResNet-18 are retrained to have top1 and top5 error as 30.23% and 10.91%. We train 200 epochs for each model. Since there exists 2 stride convolution layers in ResNet-18, we adopt max pooling operation on the adjusted importance map $\mathbf{F}_{\text{adjusted}}$ for different sizes of feature maps. For ResNet-18, we generate 4 different important maps $\mathbf{F}_{\downarrow 2}$, $\mathbf{F}_{\downarrow 4}$, $\mathbf{F}_{\downarrow 8}$, and $\mathbf{F}_{\downarrow 16}$. The final L_{sparse} is defined by a average sum of l_1 -norm on these four maps. We set $\lambda = 2.5e - 1$ and the sparse controlling factor CF can be randomized from $\{-1, 0, 1\}$ during training to support 3 levels of sparsity. Several models without ASC module is also trained with different λ settings. We compare our methods with other pruning or dynamic execution methods. [15, 29, 46, 16, 6, 18, 8].

Test results. The results can be seen in Table 4. By applying our method, only a slightly top-1 and top-5 accuracy drop with a 1.4-2.1X MACs saving can achieved.

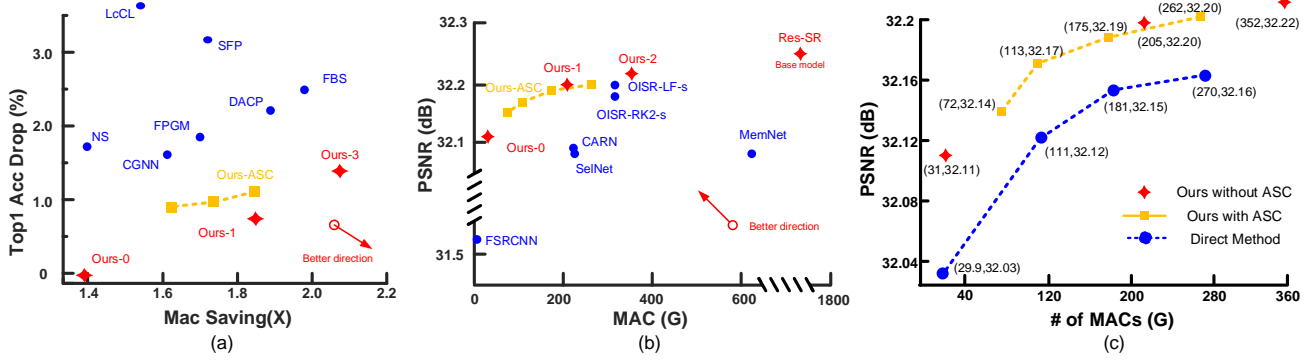


Figure 6. (a) TOP1 Acc Drop/MAC trade-off for classification tasks (b) PSNR/MAC trade-off tested on BSD100 (c) Ablation study for ASC module on super resolution tested on BSD100

Our method can achieve better results than previous fixed weight pruning methods or dynamic execution methods. A clear Top1 accuracy drop/MAC Saving trade-off is shown on Fig. 6. The proposed model has refined pixel-wise sparsity to improve the accuracy compared with the layer-wise sparse model CGNN [18] and pixel-wise model LCCL [6]. Also, our method can effectively provide the online sparse control service.

4.3. Ablation Study

4.3.1 Importance Map Network

We do ablation study on the structure of importance map network. For our previous experiments, the super resolution task has four convolution layers with 32 channels in between and the classification task has three convolution layers where it first expands to 18 layers and then comes up to 36 layers. We claim that the design of IMN module can be light-weight so that it will only cause little extra latency. We train multiple models with different structures. All the contrast experiments are done on the same hyper parameters settings. As it can be seen in Table. 3, different structures of IMN module can lead to little difference for final results. Therefore, there is no need to search the best structure. The latency caused by IMN module is negligible compared to the main functional network.

4.3.2 Automatic Sparse Controlling Network

Normally, models trained with specific sparse level can have better performance than the one that can online generate multiple sparse levels. It would be unworthy if the accuracy/latency trade-off deteriorate much with the integration of ASC module. The contrast results can be seen on Fig. 6. Our ASC module can maintain the performance with the bonus of automatic sparse controlling, which validate its worthiness. The final PSNR seems no difference for super resolution. Accuracy on classification may have some little

drop while the performance is still promising. In addition, to validate the effectiveness of our design, we compare our ASC module to another sparse control method, which directly increase or decrease numbers of channels for all the feature map. Fig. 6 shows that the proposed ASC method can be more effective to improve the final model accuracy by more than 0.05 dB compared with the native way. A possible explanation for the success is that our ASC method takes the statistical distribution of pixel importance into account and the learning way helps it to automatically find the best adjusted distribution to trade off between the sparsity and accuracy properly.

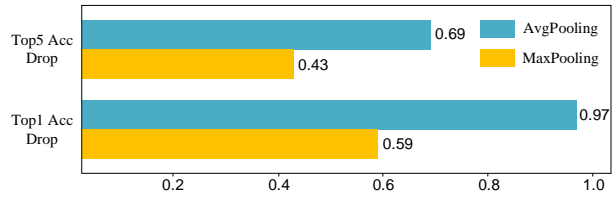


Figure 7. Ablation study for different down-sampling strategies.

4.3.3 Integration Strategy

When the feature map is reshaped, our \mathbf{M} should have a corresponding adaptation. As is mentioned in the methodology section, most of the conditions can be handled easily except the one \mathbf{F} needs to be down-sampled. Since the feature map encounters four down-sampling in ResNet-18, we do our ablation study on the image classification tasks. we study three down-sampling methods: max pooling, average pooling, and stride-2 convolutions. We find that the former two methods can be much easier trained than the latter one. One possible explanation is that the stride-2 convolution will generate several importance maps with different distributions, thus it is difficulty to find the best weights on these maps as they are summed up together to form the $\mathcal{L}_{\text{sparse}}$. Therefore,

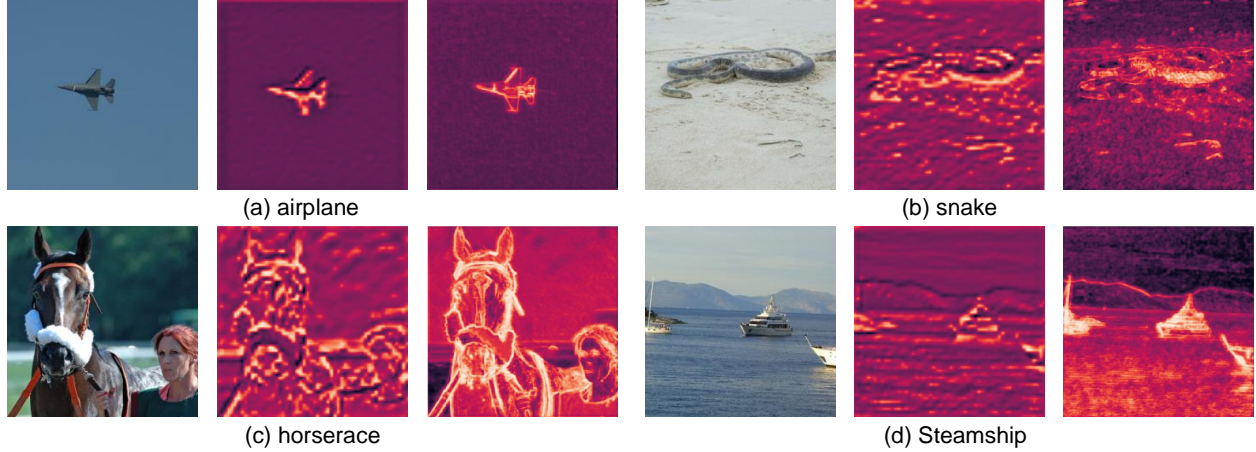


Figure 8. Input and their corresponding importance map from different tasks under similar sparsity level. The left one is from the image classification task and the right one comes from super resolution.

the latency/accuracy trade-off tends to be worse than the former two methods. Fig. 7 shows that max pooling method can achieve better performance than average pooling ones at similar sparse level. Average pooling makes the sparse level identical for all feature maps, while the max pooling makes smaller feature map more dense, which can keep more information in the latter layers. It can be inferred that the latter smaller feature maps are more important than the former ones to affect the accuracy. Also, since there exists little spatial redundancy when the size of feature map becomes small (e.g., 14×14 and even 7×7), applying pixel-wise sparsity could meet more difficulty. Therefore, max pooling is adopted in this paper.

Table 4. Hardware validation on Intel Core i5-9600K and ZYNQ-7035 with number 0 as benchmark for ResNet-18

	MACs	Theo Speedup	Runtime(ms)		Real Speedup	
			i5-9600K	Zynq-7035	i5-9600K	Zynq-7035
0	1.8G	-	1450	85.2	-	-
1	0.74G	2.45X	735	39.0	1.97X	2.18X
2	0.60G	3.01X	575	31.1	2.52X	2.73X
3	0.48G	3.73X	461	24.6	3.15X	3.46X

4.4. Hardware Validation

We test the speedup of three sparse level on Intel Core i5-9600K and the results are shown in Table. 4. For fair comparison, we replace all the layers by our C code based implementations and used four threads for one running model. Since the index of zero blocks is known in advance, we can easily skip them to save computation. Our hardware implementations is simple, as the structure of our sparsity ensures that we only need the first index of zero blocks. Although the I/O bottleneck and the complexity to utilize the sparsity of the input of one layer make the realistic speedup lower than the theoretical ones, our method remain good performance. We also design a FPGA-based accelerator using

ZYNQ-7035 device and high-level synthesis (HLS) technology by Xilinx. ResNet-18 is also chosen to be the benchmark and the realistic speedup is close to the theoretical ones. The detailed description about the deployment method on FPGA is beyond the scope of this paper. Further information may be found in [35].

4.5. Algorithm Discussion

We generate the importance map from various tasks, as is shown in Fig. 8. It can be seen that they both highlight the important region of the input image. The difference is caused by the different goals of the tasks. Super resolution aims to reconstruct detailed textures. Therefore, the importance map also shows which region is hard to transform into the high resolution ones. More channels are activated in those areas to help reconstruction. Importance map in the image classification tasks works in a different way. It samples the most representative image patches to extract more semantic information. Although the importance image seems not as elaborate as the ones in super resolution tasks, we can see a refined highlight of the interested object in the image.

5. Conclusion

In this paper, we propose a novel spatially adaptive method to generate structured sparsity in CNN-based models. We adopt a pixel-wise sparse method that is dynamically adapted by an unified importance map, which achieves good performance to reduce the network computing cost while maintaining the accuracy. An adjustable mechanism to online control the sparse level in one model is also developed to avoid training multiple models for specific applications. Our method can be widely used on various CNN structure and is validated on two different vision tasks: super resolution and classification. Experimental results show that our approach

achieves high performance in both of them. Hardware validation is also implemented to prove the practical value of our method.

References

- [1] Namhyuk Ahn, Byungkun Kang, and Kyung-Ah Sohn. Fast, accurate, and lightweight super-resolution with cascading residual network. In *Proceedings of the European Conference on Computer Vision (ECCV)*, pages 252–268, 2018. 6
- [2] Marco Bevilacqua, Aline Roumy, Christine Guillemot, and Marie Line Alberi-Morel. Low-complexity single-image super-resolution based on nonnegative neighbor embedding. 2012. 5
- [3] Jae-Seok Choi and Munchurl Kim. A deep convolutional neural network with selection units for super-resolution. In *Proceedings of the IEEE conference on computer vision and pattern recognition workshops*, pages 154–160, 2017. 6
- [4] Xiaohan Ding, Guiguang Ding, Yuchen Guo, and Jungong Han. Centripetal sgD for pruning very deep convolutional networks with complicated structure. In *Proceedings of the IEEE/CVF Conference on Computer Vision and Pattern Recognition*, pages 4943–4953, 2019. 2
- [5] Chao Dong, Chen Change Loy, and Xiaoou Tang. Accelerating the super-resolution convolutional neural network. In *European conference on computer vision*, pages 391–407. Springer, 2016. 6
- [6] Xuanyi Dong, Junshi Huang, Yi Yang, and Shuicheng Yan. More is less: A more complicated network with less inference complexity. In *Proceedings of the IEEE Conference on Computer Vision and Pattern Recognition*, pages 5840–5848, 2017. 2, 3, 6, 7
- [7] Michael Figurnov, Maxwell D Collins, Yukun Zhu, Li Zhang, Jonathan Huang, Dmitry Vetrov, and Ruslan Salakhutdinov. Spatially adaptive computation time for residual networks. In *Proceedings of the IEEE Conference on Computer Vision and Pattern Recognition*, pages 1039–1048, 2017. 1, 2
- [8] Xitong Gao, Yiren Zhao, Łukasz Dudziak, Robert Mullins, and Cheng-zhong Xu. Dynamic channel pruning: Feature boosting and suppression. *arXiv preprint arXiv:1810.05331*, 2018. 2, 3, 6
- [9] Yiwen Guo, Anbang Yao, and Yurong Chen. Dynamic network surgery for efficient dnns. *arXiv preprint arXiv:1608.04493*, 2016. 1, 2
- [10] Song Han, Xingyu Liu, Huizi Mao, Jing Pu, Ardavan Pedram, Mark Horowitz, Bill Dally, et al. Deep compression and eie: Efficient inference engine on compressed deep neural network. In *Hot Chips Symposium*, pages 1–6, 2016. 1, 2
- [11] Song Han, Jeff Pool, John Tran, and William J Dally. Learning both weights and connections for efficient neural networks. *arXiv preprint arXiv:1506.02626*, 2015. 1, 2
- [12] Babak Hassibi and David G Stork. *Second order derivatives for network pruning: Optimal brain surgeon*. Morgan Kaufmann, 1993. 1, 2
- [13] Kaiming He, Xiangyu Zhang, Shaoqing Ren, and Jian Sun. Deep residual learning for image recognition. In *Proceedings of the IEEE conference on computer vision and pattern recognition*, pages 770–778, 2016. 6
- [14] Xiangyu He, Zitao Mo, Peisong Wang, Yang Liu, Mingyuan Yang, and Jian Cheng. Ode-inspired network design for single image super-resolution. In *Proceedings of the IEEE/CVF Conference on Computer Vision and Pattern Recognition*, pages 1732–1741, 2019. 6
- [15] Yang He, Guoliang Kang, Xuanyi Dong, Yanwei Fu, and Yi Yang. Soft filter pruning for accelerating deep convolutional neural networks. *arXiv preprint arXiv:1808.06866*, 2018. 6
- [16] Yang He, Ping Liu, Ziwei Wang, Zhilan Hu, and Yi Yang. Filter pruning via geometric median for deep convolutional neural networks acceleration. In *Proceedings of the IEEE/CVF Conference on Computer Vision and Pattern Recognition*, pages 4340–4349, 2019. 2, 6
- [17] Yihui He, Xiangyu Zhang, and Jian Sun. Channel pruning for accelerating very deep neural networks. In *Proceedings of the IEEE International Conference on Computer Vision*, pages 1389–1397, 2017. 1, 2
- [18] Weizhe Hua, Yuan Zhou, Christopher De Sa, Zhiru Zhang, and G Edward Suh. Channel gating neural networks. *arXiv preprint arXiv:1805.12549*, 2018. 6, 7
- [19] Jia-Bin Huang, Abhishek Singh, and Narendra Ahuja. Single image super-resolution from transformed self-exemplars. In *Proceedings of the IEEE conference on computer vision and pattern recognition*, pages 5197–5206, 2015. 5
- [20] Tao Kong, Fuchun Sun, Anbang Yao, Huaping Liu, Ming Lu, and Yurong Chen. Ron: Reverse connection with objectness prior networks for object detection. In *Proceedings of the IEEE conference on computer vision and pattern recognition*, pages 5936–5944, 2017. 2, 3
- [21] Jason Kuen, Xiangfei Kong, Zhe Lin, Gang Wang, Jianxiong Yin, Simon See, and Yap-Peng Tan. Stochastic downsampling for cost-adjustable inference and improved regularization in convolutional networks. In *Proceedings of the IEEE Conference on Computer Vision and Pattern Recognition*, pages 7929–7938, 2018. 2, 3
- [22] Christian Ledig, Lucas Theis, Ferenc Huszár, Jose Caballero, Andrew Cunningham, Alejandro Acosta, Andrew Aitken, Alykhan Tejani, Johannes Totz, Zehan Wang, et al. Photo-realistic single image super-resolution using a generative adversarial network. In *Proceedings of the IEEE conference on computer vision and pattern recognition*, pages 4681–4690, 2017. 5
- [23] Namhoon Lee, Thalaiyasingam Ajanthan, and Philip HS Torr. Snip: Single-shot network pruning based on connection sensitivity. *arXiv preprint arXiv:1810.02340*, 2018. 1, 2
- [24] Hao Li, Asim Kadav, Igor Durdanovic, Hanan Samet, and Hans Peter Graf. Pruning filters for efficient convnets. *arXiv preprint arXiv:1608.08710*, 2016. 1, 2
- [25] Juncheng Li, Faming Fang, Kangfu Mei, and Guixu Zhang. Multi-scale residual network for image super-resolution. In *Proceedings of the European Conference on Computer Vision (ECCV)*, pages 517–532, 2018. 6
- [26] Xiaoxiao Li, Ziwei Liu, Ping Luo, Chen Change Loy, and Xiaoou Tang. Not all pixels are equal: Difficulty-aware semantic segmentation via deep layer cascade. In *Proceedings of the IEEE conference on computer vision and pattern recognition*, pages 3193–3202, 2017. 1, 2, 3

- [27] Ji Lin, Yongming Rao, Jiwen Lu, and Jie Zhou. Runtime neural pruning. In *Proceedings of the 31st International Conference on Neural Information Processing Systems*, pages 2178–2188, 2017. 2, 3
- [28] Shaohui Lin, Rongrong Ji, Chenqian Yan, Baochang Zhang, Liujuan Cao, Qixiang Ye, Feiyue Huang, and David Doermann. Towards optimal structured cnn pruning via generative adversarial learning. In *Proceedings of the IEEE/CVF Conference on Computer Vision and Pattern Recognition*, pages 2790–2799, 2019. 2
- [29] Zhuang Liu, Jianguo Li, Zhiqiang Shen, Gao Huang, Shoumeng Yan, and Changshui Zhang. Learning efficient convolutional networks through network slimming. In *Proceedings of the IEEE International Conference on Computer Vision*, pages 2736–2744, 2017. 1, 2, 6
- [30] Jian-Hao Luo, Jianxin Wu, and Weiyao Lin. Thinet: A filter level pruning method for deep neural network compression. In *Proceedings of the IEEE international conference on computer vision*, pages 5058–5066, 2017. 2
- [31] Xiaolong Ma, Fu-Ming Guo, Wei Niu, Xue Lin, Jian Tang, Kaisheng Ma, Bin Ren, and Yanzhi Wang. Pconv: The missing but desirable sparsity in dnn weight pruning for real-time execution on mobile devices. In *Proceedings of the AAAI Conference on Artificial Intelligence*, volume 34, pages 5117–5124, 2020. 2
- [32] David Martin, Charless Fowlkes, Doron Tal, and Jitendra Malik. A database of human segmented natural images and its application to evaluating segmentation algorithms and measuring ecological statistics. In *Proceedings Eighth IEEE International Conference on Computer Vision. ICCV 2001*, volume 2, pages 416–423. IEEE, 2001. 5
- [33] Mengye Ren, Andrei Pokrovsky, Bin Yang, and Raquel Urtasun. Sbnnet: Sparse blocks network for fast inference. In *Proceedings of the IEEE Conference on Computer Vision and Pattern Recognition*, pages 8711–8720, 2018. 2, 3
- [34] Olga Russakovsky, Jia Deng, Hao Su, Jonathan Krause, Sanjeev Satheesh, Sean Ma, Zhiheng Huang, Andrej Karpathy, Aditya Khosla, Michael Bernstein, et al. Imagenet large scale visual recognition challenge. *International journal of computer vision*, 115(3):211–252, 2015. 6
- [35] Wenyu Sun, Chen Tang, Zhuqing Yuan, Zhe Yuan, Huazhong Yang, and Yongpan Liu. A 112-765 gops/w fpga-based cnn accelerator using importance map guided adaptive activation sparsification for pix2pix applications. In *2020 IEEE Asian Solid-State Circuits Conference (A-SSCC)*, pages 1–4. IEEE, 2020. 8
- [36] Ying Tai, Jian Yang, and Xiaoming Liu. Image super-resolution via deep recursive residual network. In *Proceedings of the IEEE conference on computer vision and pattern recognition*, pages 3147–3155, 2017. 6
- [37] Ying Tai, Jian Yang, Xiaoming Liu, and Chunyan Xu. Memnet: A persistent memory network for image restoration. In *Proceedings of the IEEE international conference on computer vision*, pages 4539–4547, 2017. 6
- [38] Radu Timofte, Eirikur Agustsson, Luc Van Gool, Ming-Hsuan Yang, and Lei Zhang. Ntire 2017 challenge on single image super-resolution: Methods and results. In *Proceedings of the IEEE conference on computer vision and pattern recognition workshops*, pages 114–125, 2017. 5
- [39] Andreas Veit and Serge Belongie. Convolutional networks with adaptive inference graphs. In *Proceedings of the European Conference on Computer Vision (ECCV)*, pages 3–18, 2018. 1, 2, 3
- [40] Jingyu Wang, Songming Yu, Jinshan Yue, Zhe Yuan, Zhuqing Yuan, Huazhong Yang, Xueqing Li, and Yongpan Liu. High pe utilization cnn accelerator with channel fusion supporting pattern-compressed sparse neural networks. In *2020 57th ACM/IEEE Design Automation Conference (DAC)*, pages 1–6. IEEE, 2020. 2
- [41] Zhou Wang, Alan C Bovik, Hamid R Sheikh, and Eero P Simoncelli. Image quality assessment: from error visibility to structural similarity. *IEEE transactions on image processing*, 13(4):600–612, 2004. 5
- [42] Wei Wen, Chunpeng Wu, Yandan Wang, Yiran Chen, and Hai Li. Learning structured sparsity in deep neural networks. *arXiv preprint arXiv:1608.03665*, 2016. 2
- [43] Zhenda Xie, Zheng Zhang, Xizhou Zhu, Gao Huang, and Stephen Lin. Spatially adaptive inference with stochastic feature sampling and interpolation. In *European Conference on Computer Vision*, pages 531–548. Springer, 2020. 2, 3
- [44] Jianbo Ye, Xin Lu, Zhe Lin, and James Z Wang. Rethinking the smaller-norm-less-informative assumption in channel pruning of convolution layers. *arXiv preprint arXiv:1802.00124*, 2018. 2
- [45] Roman Zeyde, Michael Elad, and Matan Protter. On single image scale-up using sparse-representations. In *International conference on curves and surfaces*, pages 711–730. Springer, 2010. 5
- [46] Zhuangwei Zhuang, Mingkui Tan, Bohan Zhuang, Jing Liu, Yong Guo, Qingyao Wu, Junzhou Huang, and Jinhui Zhu. Discrimination-aware channel pruning for deep neural networks. *arXiv preprint arXiv:1810.11809*, 2018. 2, 6